

Highly Luminous N³⁻-Substituted Li₂MSiO_{4-δ}N_{2/3δ}:Eu²⁺ (M = Ca, Sr, and Ba) for White NUV Light-Emitting Diodes

Donghyeon Kim,[†] Choon Woo Ji,^{‡,#} Jungjun Lee,[‡] Jong-Seong Bae,[§] Tae Eun Hong,[§] Sung Il Ahn,^{||} In Chung,[‡] Seung-Joo Kim,^{*,†} and Jung-Chul Park^{*,†}

[†]Department of Energy Systems Research and Department of Chemistry, Ajou University, Suwon 16499, Republic of Korea

[‡]Center for Green Fusion Technology and Department of Engineering in Energy & Applied Chemistry, Silla University, Busan 46958, Republic of Korea

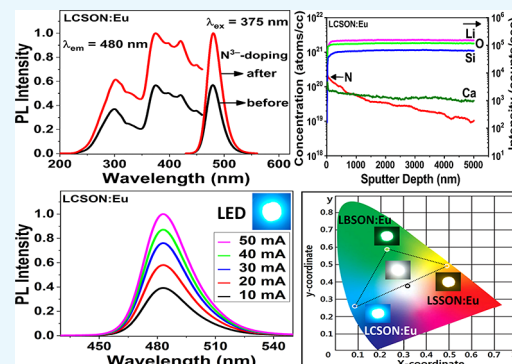
[§]Busan Center, Korea Basic Science Institute, Busan 46742, Republic of Korea

^{||}Department of Chemistry Education, Pusan National University, Busan 46241, Republic of Korea

^{*}School of Chemical and Biological Engineering, Seoul National University, Seoul 08826, Republic of Korea

Supporting Information

ABSTRACT: The N³⁻-substituted Li₂MSiO₄:Eu²⁺ (M = Ca, Sr, and Ba) phosphors were systematically prepared and analyzed. Secondary-ion mass spectroscopy measurements revealed that the average N³⁻ contents are 0.003 for Ca, 0.009 for Sr, and 0.032 for Ba. Furthermore, the N³⁻ incorporation in the host lattices was corroborated by infrared and X-ray photoelectron spectroscopies. From the photoluminescence spectra of Li₂MSiO₄:Eu²⁺ (M = Ca, Sr, and Ba) phosphors before and after N³⁻ doping, it was verified that the enhanced emission intensity of the phosphors is most likely due to the N³⁻ doping. In Li₂MSiO₄:Eu²⁺ (M = Ca, Sr, and Ba) phosphors, the maximum wavelengths of the emission band were red-shifted in the order Ca < Ba < Sr, which is not consistent with the trend of crystal field splitting: Ba < Sr < Ca. This discrepancy was clearly explained by electron–electron repulsions among polyhedra, LiO₄–MO_n, SiO₄–MO_n, and MO_n–M' O_n associated with structural difference in the host lattices. Therefore, the energy levels associated with the 4f⁶5d energy levels of Eu²⁺ are definitely established in the following order: Li₂CaSiO₄:Eu²⁺ > Li₂BaSiO₄:Eu²⁺ > Li₂SrSiO₄:Eu²⁺. Furthermore, using the Williamson–Hall (W–H) method, the determined structural strains of Li₂MSiO₄:Eu²⁺ (M = Ca, Sr, and Ba) phosphors revealed that the increased compressive strain after N³⁻ doping induces the enhanced emission intensity of these phosphors. White light-emitting diodes made by three N³⁻-doped phosphors and a 365 nm emitting InGaN chip showed the (0.333, 0.373) color coordinate and high color-rendering index ($R_a = 83$). These phosphor materials may provide a platform for development of new efficient phosphors in solid-state lighting field.



INTRODUCTION

Recently, many researchers have focused their attention on rare-earth-doped phosphor materials for solid-state lighting, especially in white light-emitting diodes (w-LEDs). Commercialized w-LEDs are made up of a blue-emitting LED chip and a yellow-emitting phosphor (Y₃Al₅O₁₂:Ce³⁺ (YAG:Ce)). However, they exhibit a low color-rendering index (CRI) because they generate weak red emission.¹ To solve the problem, optimal phosphors should be newly developed. Therefore, new classes of phosphors based on metal silicates, metal sulfides, metal oxy-nitrides, and metal nitrides have been developed.^{2–9} Liu et al. reported that Li₂CaSiO₄:Eu²⁺ (with a tetragonal phase, space group $I\bar{4}2m$) has high absorption from the UV to the near-UV region and a strong emission at ~480 nm with a narrow bandwidth.⁹ Orange-yellow-emitting Li₂SrSiO₄:Eu²⁺ (with a trigonal crystal system and belonging to space group $P3_121$) was prepared and compared to the commercialized YAG:Ce phosphor by Varadaraju et al.¹⁰

Recently, the crystal structure and PL properties of Eu²⁺-doped Li₂BaSiO₄ have been elucidated and discussed by Kulshreshtha et al.¹¹ and Kim et al.,¹² i.e., the hexagonal crystal system (belonging to space group $P6_3cm$) and green emission at ~508 nm, respectively. Based on the structures of the host materials in Li₂MSiO₄ (M = Ca, Sr, and Ba), it is presumed that the luminescent properties of these phosphor materials may be closely related to the chemical environment around the Eu²⁺-activator ion. It is well known that alkaline-earth silicon-oxy-nitride phosphors with the RE-ion activator (RE = Ce³⁺, Eu²⁺, Yb³⁺, etc.) have been intensively studied in recent years because they are potential candidate materials for improving the low luminous efficiency and low CRI for w-LEDs.^{13–16} The N³⁻ ions substituted partially for O²⁻ ions in the host

Received: January 19, 2019

Accepted: April 16, 2019

Published: May 13, 2019



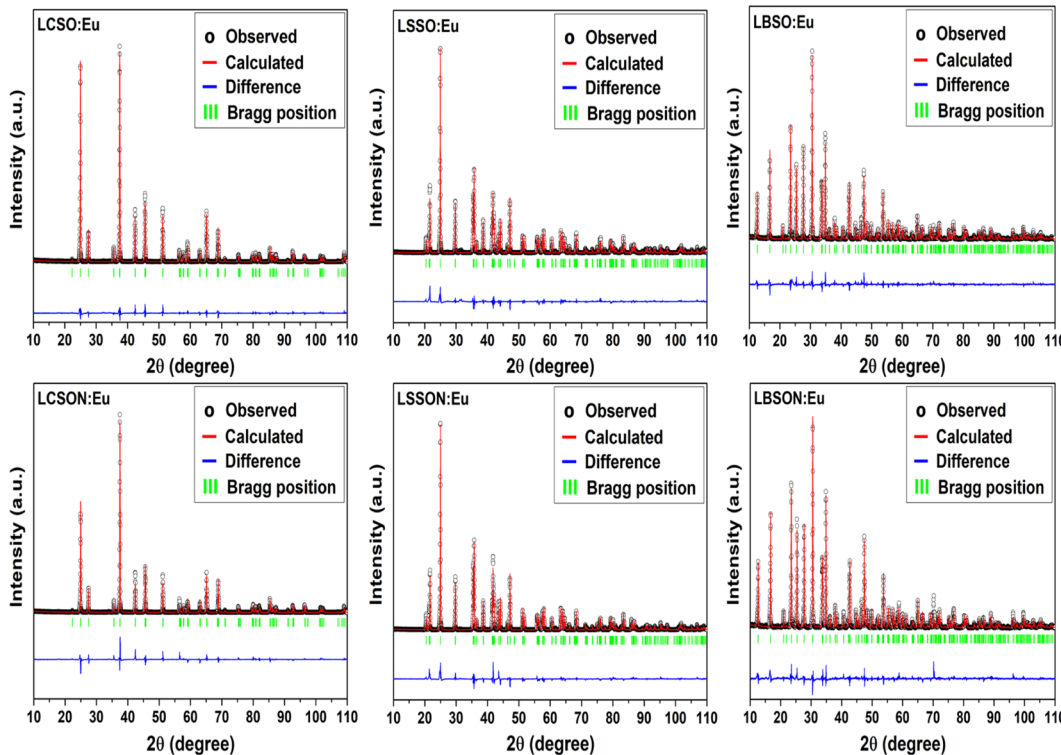


Figure 1. Rietveld refinement profile of the powder XRD data for LCSO:Eu, LSSO:Eu, and LBSO:Eu before and after N^{3-} doping. The measured, fitted data, expected reflection positions, and difference between the measured and fitted data are depicted as black circles, red lines, green lines, and blue lines, respectively.

lattice could change the electronic structure of Eu^{2+} owing to their difference in electronegativity, ionic radius, and magnitude of crystal field splitting, as well as the nephelauxetic (cloud expanding) effect of the two ions,^{3,17} which results in the change of the PL properties of the phosphors before and after N^{3-} doping. Song et al. mentioned that the partial nitridation of $\text{Li}_2\text{SrSiO}_{4-3x/2}\text{N}_x\text{:Eu}^{2+}$ ($x = 0.01$) phosphors induced a highly enhanced PL intensity by as high as 190%.¹⁸ Therefore, it is presumed that their results for the N^{3-} doping effect on an increase of the luminescent intensity are meaningful even though the N^{3-} contents doped into the crystal sites were not determined. However, systematic research for the N^{3-} doping effect of Li_2MSiO_4 ($M = \text{Ca}$ and Ba) has not been pursued to the best of our knowledge. Furthermore, the present study is also motivated by the desire to devise a white near-UV LED because Eu^{2+} -activated Li_2MSiO_4 ($M = \text{Ca}$, Sr , and Ba) phosphors exhibit blue, orange-yellow, and green emission, respectively. Herein, we report on the highly enhanced luminescence of N^{3-} -substituted $\text{Li}_2\text{MSiO}_4\text{:Eu}^{2+}$ ($M = \text{Ca}$, Sr , and Ba) and a white near-UV LED using three phosphors.

RESULTS AND DISCUSSION

Characterization of Crystal Structure. The crystal structure of each compound was characterized by its X-ray diffraction (XRD) pattern using the Rietveld method¹⁹ with the FullProf program.²⁰ From the ICSD database, the equivalent isotropic displacement parameters and atomic coordinates were used. Using a pseudo-Voigt function with an asymmetry correction at low angles, the shape of the peak was fitted. The obtained patterns from Rietveld refinement of the XRD data are presented in Figure 1. The final values of the

equivalent isotropic displacement parameters and atomic coordinates are given in Table S1 (and Tables S3 and S5). The selected bond distances are presented in Table S2 (and Tables S4 and S6). Figure 2 shows the change in lattice volume before and after the nitridation of each Li_2MSiO_4 compound.

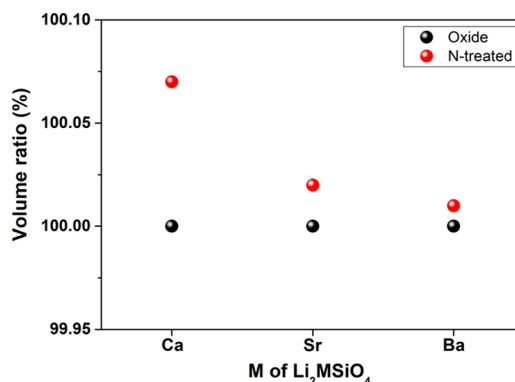


Figure 2. Lattice volume changes before and after N^{3-} doping of each $\text{Li}_2\text{MSiO}_4\text{:Eu}$ ($M = \text{Ca}$, Sr , and Ba) compound.

Determination of N^{3-} Contents by Secondary-Ion Mass Spectroscopy. To determine the N^{3-} contents of $\text{Li}_2\text{CaSiO}_{4-\delta}\text{N}_{2/3\delta}$ (LCSON), $\text{Li}_2\text{SrSiO}_{4-\delta}\text{N}_{2/3\delta}$ (LSSON), and $\text{Li}_2\text{BaSiO}_{4-\delta}\text{N}_{2/3\delta}$ (LBSON), secondary-ion mass spectrometry (SIMS) analysis was used. It is well known that SIMS gives the best detection limit for identifying elements with very low concentrations compared to other techniques in surface analysis area. The elemental composition using SIMS can be quantitatively determined with an ion-implanted standard material.^{3,21,22} Figure 3 shows the atomic intensity and

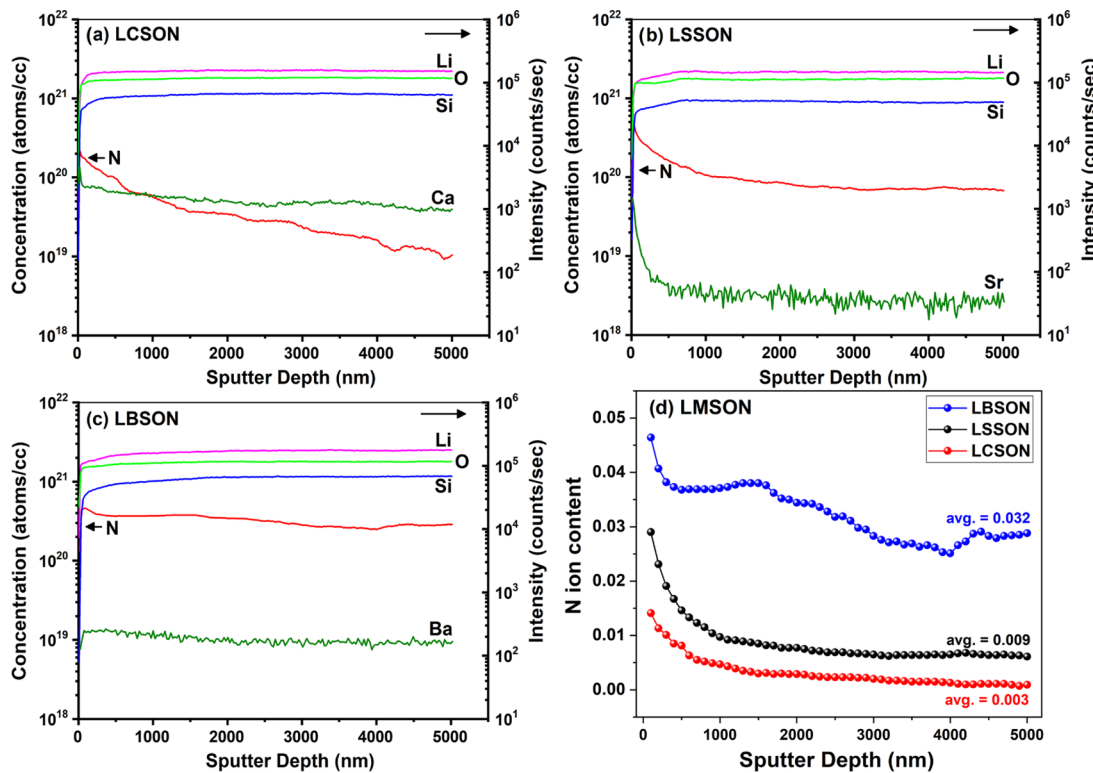


Figure 3. Atomic intensity and concentration versus sputter depth of LCSON (a), LSSON (b), LBSON (c), and N^{3-} contents (d) by SIMS measurements.

concentration versus the sputter depth of the compounds. For Li, Si, and O atoms among the three phosphors, no difference in the secondary-ion intensities was observed, while the intensities of secondary-ion for Ca, Sr, and Ba atoms changed because of the different sensitivities of the elements. The concentrations of N atom are analyzed as a function of sputter depth from the surface to the inner region of the grains (~ 5000 nm) for the three samples. The contents of N^{3-} ion were calculated as shown in Figure 3d. The average contents of N^{3-} ion for LCSON, LSSON, and LBSON were 0.003, 0.009, and 0.032, respectively. It is remarkable that the N^{3-} -ion content increases with larger alkaline-earth metal-ion size ($\text{Ba}^{2+} > \text{Sr}^{2+} > \text{Ca}^{2+}$), probably implying that $\text{Li}_2\text{MSiO}_{4-\delta}\text{N}_{2/3\delta}\text{Eu}^{2+}$ ($\text{M} = \text{Ca}, \text{Sr}, \text{and Ba}$) phosphors with the larger ion size can easily accommodate more N^{3-} ions in the crystal sites. The framework of the Li_2MSiO_4 ($\text{M} = \text{Ca}, \text{Sr}, \text{and Ba}$) structure is connected by SiO_4 and LiO_4 tetrahedra with M^{2+} ions, where two SiO_4 and LiO_4 tetrahedra are linked through sharing of oxygen atoms. Therefore, the bond lengths of MO_n polyhedra may be affected by the N^{3-} content introduced into the host lattice. The average bond distances for the three compounds (see Tables S2, S4, and S6) were determined as 2.535 Å for LCSON, 2.625 Å for LSSON, and 2.877 Å for LBSON.

Evidence of N^{3-} Incorporated in the Host Lattice from Infrared and X-ray Photoelectron Spectroscopy Measurements. The infrared (IR) spectra of Li_2MSiO_4 ($\text{M} = \text{Ca}, \text{Sr}, \text{and Ba}$) compounds before and after N^{3-} doping are shown in Figure 4. As the chemical bond of $\text{Si}-\text{O}$ is stronger than that of $\text{M}-\text{O}$ ($\text{M} = \text{Li}, \text{Ca}, \text{Sr}, \text{and Ba}$), the internal vibrations of SiO_4 tetrahedra are nearly independent of the lattice vibrations and exclusively observed in the 400–1000 cm^{-1} range. As shown in Figure 4, the $[\text{SiO}_4]$ internal modes are assigned to the $\text{Si}-\text{O}$ stretching modes^{23–25} between 770

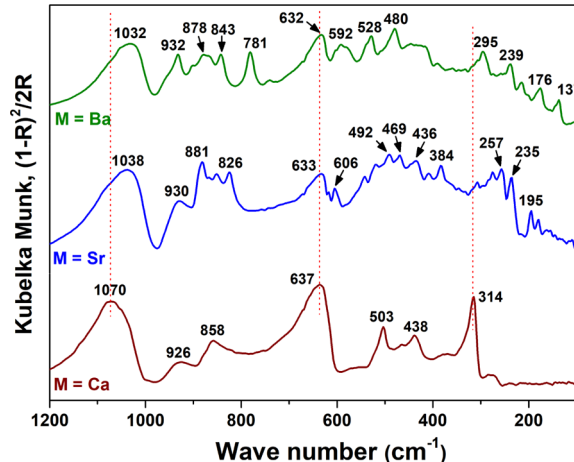


Figure 4. Fourier-transform infrared (FT-IR) spectra of the $\text{Li}_2\text{MSiO}_4:\text{Eu}$ ($\text{M} = \text{Ca}, \text{Sr}, \text{and Ba}$) compound.

and 950 cm^{-1} and to the $\text{O}-\text{Si}-\text{O}$ bending modes^{26,27} between 400 and 560 cm^{-1} . Furthermore, based on the far-IR modes of MCO_3 ($\text{M} = \text{Ca}, \text{Sr}, \text{and Ba}$) (Figure S1), the force constant (K) of $\text{M}-\text{O}$,²⁸ the reduced mass (μ) of $\text{M}-\text{O}$ ($\mu = 11.43$ for $\text{Ca}-\text{O}$, $\mu = 13.53$ for $\text{Sr}-\text{O}$, $\mu = 14.33$ for $\text{Ba}-\text{O}$), and the $\text{M}-\text{O}$ stretching modes are estimated to be 314 cm^{-1} for $\text{Ca}-\text{O}$ stretching, 257 cm^{-1} for $\text{Sr}-\text{O}$ stretching, and 239 cm^{-1} for $\text{Ba}-\text{O}$ stretching. Remarkably, the $\text{Si}-\text{O}$ stretching modes between 770 and 950 cm^{-1} are somewhat decreased after N^{3-} doping, which implies that the N^{3-} ions are partially substituted into the Li_2MSiO_4 ($\text{M} = \text{Ca}, \text{Sr}, \text{and Ba}$) host lattice. The Gaussian-fitted IR modes of LSSO and LSSON between 1100 and 770 cm^{-1} (Figure 5) corroborate the presence of N^{3-} ions substituted into the host lattice, i.e., after

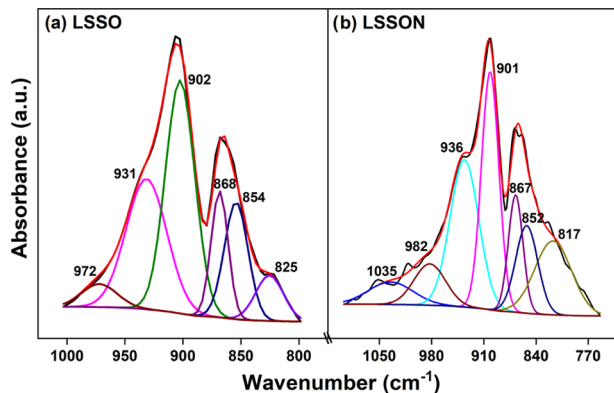


Figure 5. Gaussian-fitted IR bands of LSSO (a) and LSSON (b) between 1100 and 750 cm⁻¹.

N³⁻ doping, the sub-band centered at 825 cm⁻¹ shifts to the band with a maximum at 817 cm⁻¹. This chemical shift can be easily explained by a comparison of the chemical bond distance (1.62 Å for SiO₂ and 1.73 Å for α -Si₃N₄)^{29,30} and the chemical bond energy (454 kJ/mol for SiO₂ and 426 kJ/mol for α -Si₃N₄)³¹ between SiO₂ and α -Si₃N₄. X-ray photoelectron spectroscopy (XPS) results warrant the evidence of N³⁻ doping, closely related to the red shift of the Si–O stretching modes (from IR measurement) in these compounds. Figure 6 shows Si 2p (ref SiO₂, ref α -Si₃N₄, LSSO, and LSSON) and N 1s (LSSO and LSSON) XPS binding energies. All XPS patterns were fitted after a Shirley background correction. As presented in Figure 6, the Si 2p binding energy (ref SiO₂) is 102.8 eV with a single Gaussian band (Full width at half-maximum = 1.9 eV), whereas the Si 2p binding energies (ref α -Si₃N₄) is composed of two bands (101.4 and 102.8 eV). In the Si 2p binding energy (ref α -Si₃N₄), the sub-band at 102.8 eV may be due to superficial oxidation. The Gaussian-fitted LSSO and LSSON XPS images (middle) reveal that the Si 2p binding energy of LSSON (100.7 eV) is lower than that of LSSO (101.5 eV), which means that the N³⁻ ions are partially substituted into the LSSO crystal lattice. Furthermore, the N 1s binding energy (393.4 eV) of LSSON corroborates the N³⁻ introduction in the LSSO host lattice.

Photoluminescence Monitored under UV Light.

Figure 7 presents photoluminescence (PL) spectra of Li₂MSiO₄:Eu²⁺ (M = Ca, Sr, and Ba) before and after N³⁻ doping. The excitation spectra of the three phosphors are somewhat different in shape, probably because of the distinct crystal system of host lattices: tetragonal for Li₂CaSiO₄, trigonal for Li₂SrSiO₄, and hexagonal for Li₂BaSiO₄. For Ca and Sr, the emission intensities are increased after N³⁻ doping, by factors of 1.8 and 1.5, respectively. For Ba, there is no considerable increase even after N³⁻ doping. The emission spectra exhibit broad bands with band maxima between 450 and 650 nm: 480 nm for Ca, 569 nm for Sr, and 509 nm for Ba. The 4f–5d transition energy of Eu²⁺ is greatly dependent on the local environment because the local structure around Eu²⁺-activator ion has a great influence on the centroid shift energy (CS) and crystal field splitting (CFS) of the 5d levels as well as the Stokes shift (ΔS) of the emission. Among the factors determining the 4f–5d transition energy of Eu²⁺, the center of gravity (barycenter) of the 5d levels is lowered relative to the free Eu²⁺ in the vacuum state, mainly ascribed to the covalent bonding character between Eu²⁺ and coordinating anions (O²⁻). Separately from a centroid shift, the neighboring anions have an additional influence on the 4f⁶5d¹ energy level of Eu²⁺, known as crystal field splitting (CFS). The magnitude of the CFS is dependent on the geometrical interaction between 5d orbitals and anion ligands: the energy of the 5d electron is raised because of the larger repulsion between the 5d electron in an orbital oriented toward an anion ligand and the electrons in the neighboring ligands, whereas that of the 5d electron in an orbital oriented away from an anion ligand is lowered. It should be mentioned that Pauling's rule 3 based on the hard-spheres electrostatic model³² states that the sharing of edge and face by two polyhedrons decreases the stability of an ionic structure because of the increase in cation–cation repulsions as the cations get close together. For a certain coordination geometry, the degree of cation–cation repulsions also increases in the following order: corner-shared < edge-shared < face-shared. Thus, Pauling's rule 3 means that most ionic solids will prefer to be corner-shared rather than edge- or face-shared because of the bond stability. Notably, Morrison verified that the shift of the central energy of 4fⁱ⁻¹5d

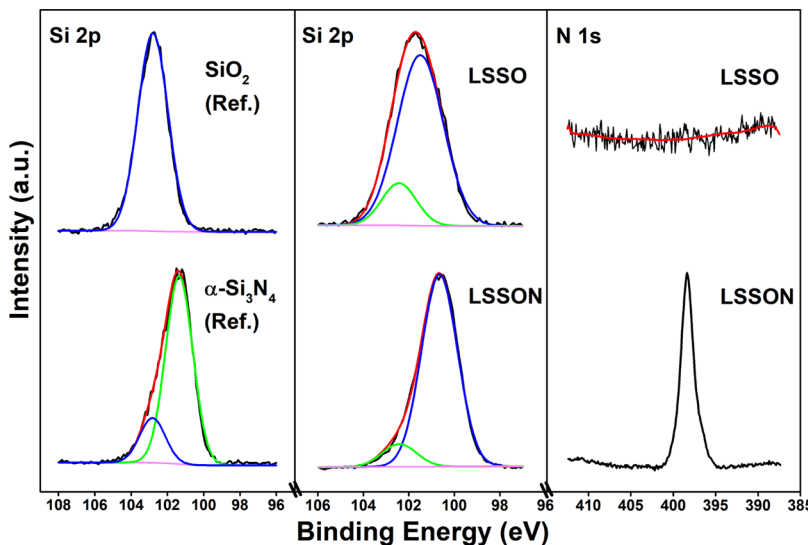


Figure 6. Si 2p and N 1s binding energies of SiO₂, α -Si₃N₄, LSSO, and LSSON using XPS.

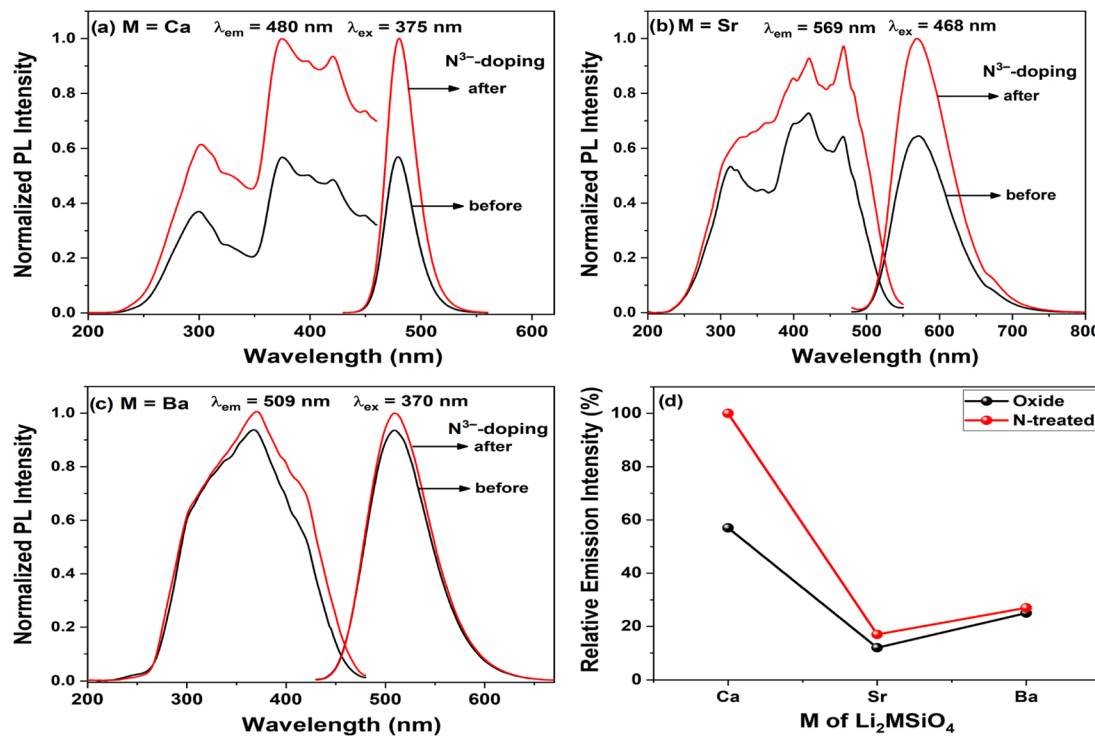


Figure 7. PL spectra of Li₂MSiO₄:Eu (M = Ca, Sr, and Ba) compound before and after N³⁻ doping; M = Ca (a), M = Sr (b), M = Ba (c), relative emission intensity (d).

configurations (for activator ion) is directly proportional to the summation of ligand polarizabilities over all nearest coordinating anion ligands.³³ Shi et al. reported that the barycenter energy of 4P¹-5d configuration on Eu²⁺ ions is strongly dependent on the environmental factor (h_e)

$$h_e = (Nf_c \alpha Q^2)^{1/2} \quad (1)$$

where N is the number of ligands, f_c is the average fractional covalence, Q is the charge of the nearest anion, and α is the average bond volume polarizability.³⁴

Therefore, the clear explanation for the wavelength shift of the emission band maxima in Li₂MSiO₄:Eu²⁺ (M = Ca, Sr, and Ba) requires reconsideration of the structural aspects of the compounds because the energy levels of Eu²⁺ are perturbed by neighbor cations and anions, such as O²⁻, Si⁴⁺, Li⁺, and M²⁺ (M = Ca, Sr, and Ba). Figure 8 shows the bonding types between a MO_n polyhedron and SiO₄ (or LiO₄) tetrahedra in Li₂MSiO₄:Eu²⁺ (M = Ca, Sr, and Ba). For example, if one assumes that the Eu²⁺ activator occupies the Ca1 site in a CaO₈ polyhedron, the repulsion between Eu²⁺ and Si⁴⁺ (or Li⁺) is more prominent than that from the neighbor CaO₈ polyhedra ($\times 8$) with corner-sharing through O atoms because of the difference in the bond distance between Ca-O and Si-O (or Li-O). As shown in Figure 8, a MO_n polyhedron is connected by SiO₄ tetrahedra, LiO₄ tetrahedra, and M'O_n polyhedra with shared corners, edges, and faces depending on the crystal structure in Li₂MSiO₄:Eu²⁺ (M = Ca, Sr, and Ba). According to Pauling's rule 3, in the only corner-shared polyhedra, the cations (or anions) are away from each other, while the distances between the cations (or anions) are getting shorter from edge-shared to face-shared, which finally results in the more enhanced electron-electron repulsions. Consequently, the energy levels of the Eu²⁺ activator stabilized in a MO_n polyhedron are perturbed and changed depending on the

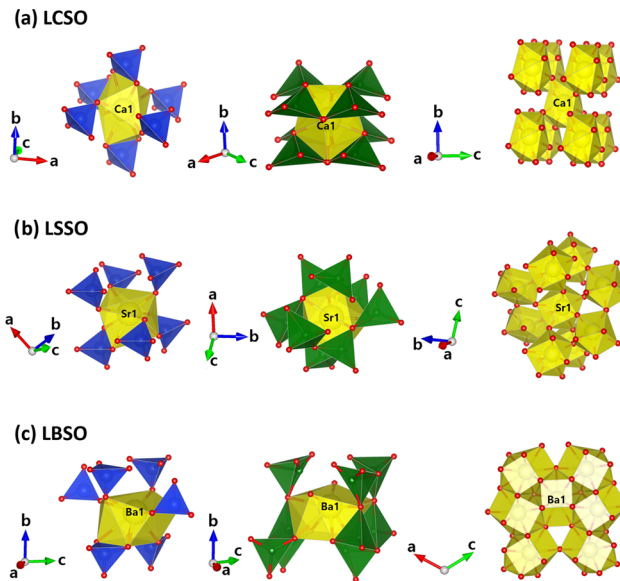


Figure 8. Local structures of Li₂MSiO₄:Eu (M = Ca, Sr, and Ba) with a fixed M1O_n-polyhedron connected by neighbor polyhedra (SiO₄-tetrahedra, LiO₄-tetrahedra, and M'O_n-polyhedra); LCSO (a), LSSO (b), and LBSO (c). Blue, green, and yellow colors represent SiO₄-tetrahedron, LiO₄-tetrahedron, and MO_n-polyhedron, respectively.

electron-electron repulsions between neighbor anions and Eu²⁺. Table 1 presents the bonding type between an AO₄ tetrahedron (A = Li and Si) and a MO_n polyhedron (M = Ca, Sr, and Ba). From the qualitative estimation of Table 1, the energy order of the 5d energy levels (Eu²⁺) can be determined as follows

$$\text{Li}_2\text{CaSiO}_4: \text{Eu}^{2+} > \text{Li}_2\text{BaSiO}_4: \text{Eu}^{2+} > \text{Li}_2\text{SrSiO}_4: \text{Eu}^{2+} \quad (2)$$

Table 1. Bonding Characteristic of $\text{Li}_2\text{MSiO}_4:\text{Eu}$ ($\text{M} = \text{Ca}, \text{Sr}, \text{and Ba}$) between a Fixed MIO_n -Polyhedron and Neighbor Polyhedra (SiO_4 -Tetrahedra, LiO_4 -Tetrahedra, and $\text{M}'\text{O}_n$ -Polyhedra)^a

	SiO_4 -tetrahedron		LiO_4 -tetrahedron		MO_n -polyhedron	
	bonding type	bond length (Å)	bonding type	bond length (Å)	bonding type	bond length (Å)
Ca1O ₈ in $\text{Li}_2\text{CaSiO}_4$	C-sharing (x4)	Ca1–Si = 3.566	E-sharing (x8)	Ca1–Li = 2.997	C-sharing (x8)	Ca1–Ca = 4.817
	E-sharing (x2)	Ca1–Si = 3.239				
Sr1O ₈ in $\text{Li}_2\text{SrSiO}_4$	C-sharing (x4)	Sr1–Si = 3.731	C-sharing (x4)	Sr1–Li = 3.593	C-sharing (x8)	Sr1–Sr = 4.962
	E-sharing (x2)	Sr1–Si = 3.275	E-sharing (x2)	Sr1–Li = 3.192	F-sharing (x2)	Sr1–Li = 2.532
Ba1O ₉ in $\text{Li}_2\text{BaSiO}_4$	C-sharing (x3)	Ba1–Si = 3.962	C-sharing (x5)	Ba1–Li = 4.189	C-sharing (x2)	Ba1–Ba = 6.011
	E-sharing (x3)	Ba1–Si = 3.585	E-sharing (x3)	Ba1–Li = 3.387	F-sharing (x4)	Ba1–Ba = 4.174
F-sharing (x1)						

^aC, E, and F mean corner, edge, and face, respectively.

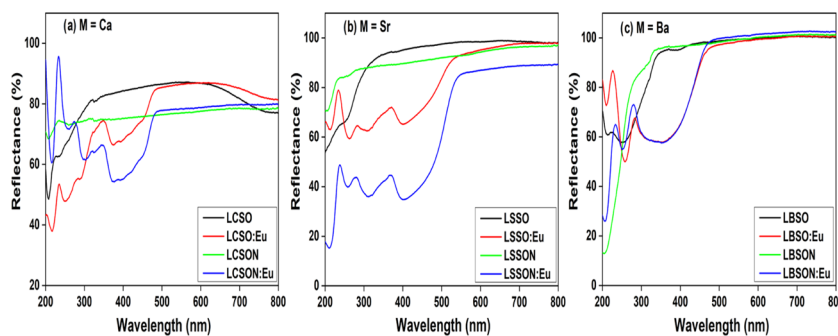


Figure 9. Diffuse reflectance spectra of LCSO:Eu (a), LSSO:Eu (b), and LBSO:Eu (c) before and after N^{3-} doping.

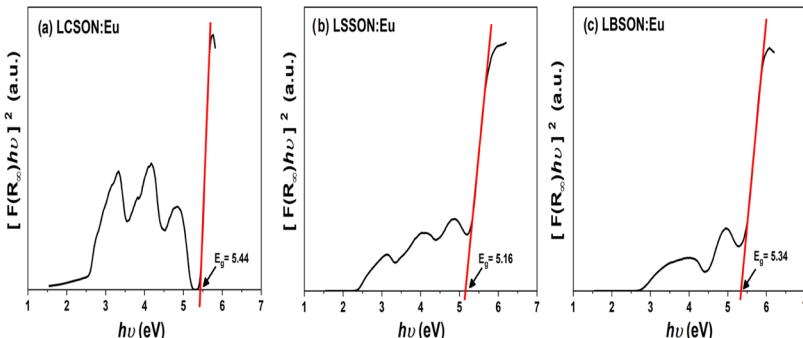


Figure 10. Band gap energies determined using the Kubelka–Munk transformation from DRS of LCSO:Eu (a), LSSO:Eu (b), and LBSO:Eu (c).

The fact that the emission spectra of $\text{Li}_2\text{MSiO}_4:\text{Eu}^{2+}$ ($\text{M} = \text{Ca}, \text{Sr}, \text{and Ba}$) (see Figure 7) show variation of the band maxima (at 480 nm for Ca, 569 nm for Sr, and 509 nm for Ba) warrants that our interpretation of the emission band maxima from Ca to Ba in these compounds is reasonable. Figure 9 presents the diffuse reflectance spectra (DRS) of $\text{Li}_2\text{MSiO}_4:\text{Eu}^{2+}$ ($\text{M} = \text{Ca}, \text{Sr}, \text{and Ba}$) before and after N^{3-} doping. It is evident that the absorption intensities between 250 and 500 nm of $\text{Li}_2\text{MSiO}_4:\text{Eu}^{2+}$ ($\text{M} = \text{Ca}, \text{Sr}, \text{and Ba}$) are greatly increased compared to those of the host lattices of Li_2MSiO_4 . Furthermore, for $\text{M} = \text{Ca}$ and Sr, the absorption bands of the N^{3-} -doped compounds are greatly intensified compared to those of $\text{Li}_2\text{MSiO}_4:\text{Eu}^{2+}$, probably as a result of the N^{3-} doping, which is in agreement with the PL results (see Figure 7). From the DRS, the band gap energies (E_g) were determined using the Kubelka–Munk transformation, and these are presented in Figure 10. It should be noted that E_g of the $\text{Li}_2\text{CaSiO}_4:\text{Eu}^{2+}$ compound was previously reported as 5.21 eV, using the Kohn–Sham density functional theory method.³⁵

In this study, we determined the following E_g values of $\text{Li}_2\text{MSiO}_4:\text{Eu}^{2+}$ ($\text{M} = \text{Ca}, \text{Sr}, \text{and Ba}$): 5.44 eV for Ca, 5.16 eV for Sr, and 5.34 eV for Ba. From band structure calculations,^{36,37} the valence band of $\text{Li}_2\text{MSiO}_4:\text{Eu}^{2+}$ ($\text{M} = \text{Ca}, \text{Sr}, \text{and Ba}$) is mainly formed by the O 2p states and the conduction band is predominantly made up of M 5d and Si 3p states. For Li_2MSiO_4 host lattices, the band gap energies progressively decrease along with $\text{Ca} \rightarrow \text{Ba} \rightarrow \text{Sr}$ because the order of energy levels of M 5d orbitals is $\text{Li}_2\text{CaSiO}_4 > \text{Li}_2\text{BaSiO}_4 > \text{Li}_2\text{SrSiO}_4$, as mentioned in the energy order of the 5d energy levels (2).

N^{3-} Doping Effect on the PL Intensity: Williamson–Hall Plot. To precisely examine the N^{3-} doping effect, the structural strain induced by the N^{3-} -doping was estimated because the ionic radius of N^{3-} (1.46 Å at CN = 4) is larger than that of O^{2-} ion (1.38 Å at CN = 4). The strain can be determined using the Williamson–Hall (W–H) method from XRD profile analysis.³⁸ The total peak width at half-maximum

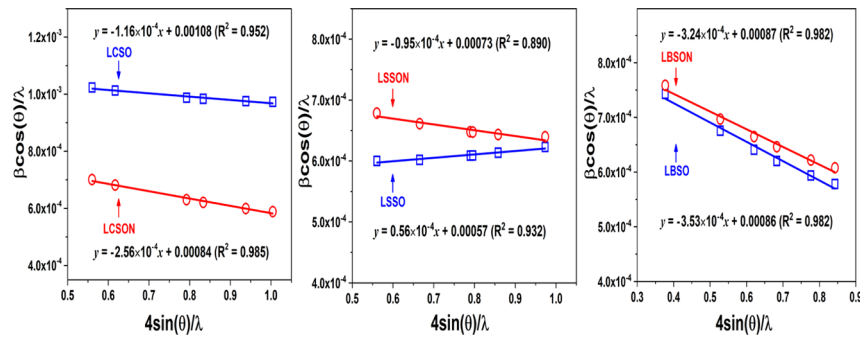


Figure 11. Williamson–Hall plots of LCSO:Eu, LSSO:Eu, and LBSO:Eu before and after N^{3-} doping.

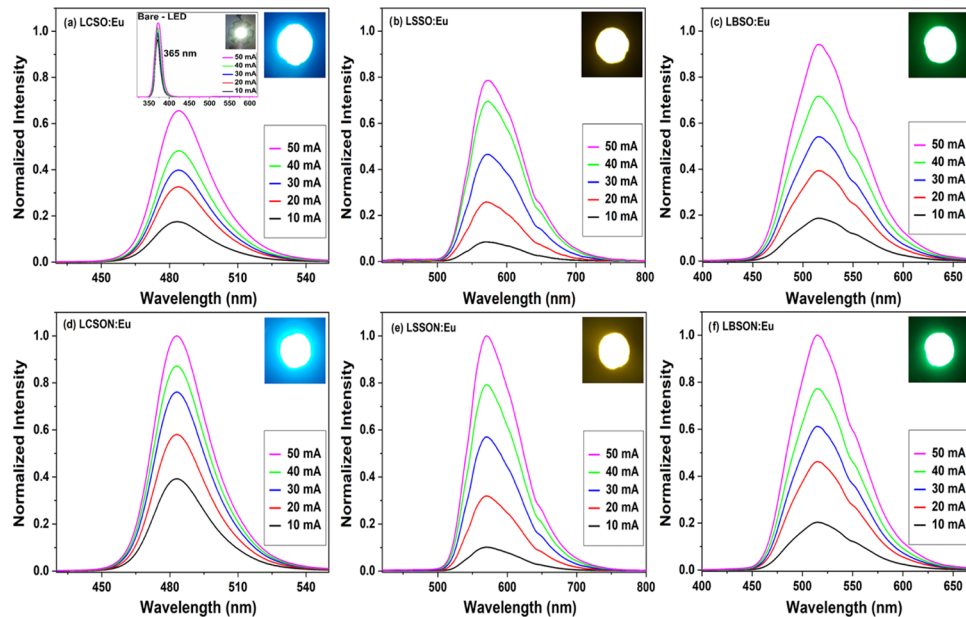


Figure 12. Photoluminescence of LEDs in the $\text{Li}_2\text{MSiO}_4:\text{Eu}$ ($\text{M} = \text{Ca}, \text{Sr}, \text{and Ba}$) compound before and after N^{3-} doping; LCSO:Eu (a), LSSO:Eu (b), LBSO:Eu (c), LCSO:Eu (d), LSSON:Eu (e), and LBSON:Eu (f).

intensity (β_{hkl}) is determined from the summation of the size broadening (β_D) and the strain broadening (β_s)

$$\beta_{hkl} = \beta_D + \beta_s \quad (3)$$

The size broadening is correlated with the Scherrer equation: $\beta_D = k\lambda/(D \cos \theta)$, where D is the crystallite size, λ is the wavelength of the X-ray, and k is the shape factor. The strain broadening is expressed by $\varepsilon = \beta_s/4 \tan \theta$, where ε is maximum strain (tensile or compressive). Thus, we get the W–H equation from eq 3

$$\beta_{hkl} \cos \theta/\lambda = k/D + 4\varepsilon \sin \theta/\lambda \quad (4)$$

The plot of $\beta_{hkl} \cos \theta/\lambda$ versus $4 \sin \theta/\lambda$ can give crystallite size from the y -intercept and strain due to lattice deformation from the slope. The W–H plots present the stain (ε) of $\text{Li}_2\text{MSiO}_4:\text{Eu}^{2+}$ ($\text{M} = \text{Ca}, \text{Sr}, \text{and Ba}$) before and after N^{3-} doping (Figure 11): for $\text{Li}_2\text{CaSiO}_4:\text{Eu}^{2+}$, from -0.012% (before N^{3-} doping, LCSO) to -0.026% (after N^{3-} doping, LCSO); for $\text{Li}_2\text{SrSiO}_4:\text{Eu}^{2+}$, from 0.0056% (before N^{3-} doping, LSSO) to -0.0095% (after N^{3-} doping, LSSON); and for $\text{Li}_2\text{BaSiO}_4:\text{Eu}^{2+}$, from -0.035% (before N^{3-} doping, LBSO) to -0.032% (after N^{3-} doping, LBSON). The positive and negative values correspond to the tensile and compressive strains, respectively. As the temperature increases, generally, a

crystal lattice undergoes tensile stress and expands. It is generally accepted that under the tensile stress, the lattice vibrations and/or the formation of defects force the phosphors more easily to promote nonradiative relaxation.^{39–41} Thus, it is presumed that the enhancement of PL intensity is ascribed to the compensation of the thermally induced tensile stress by the compressive stress due to the N^{3-} doping in $\text{Li}_2\text{MSiO}_4:\text{Eu}^{2+}$ ($\text{M} = \text{Ca}, \text{Sr}, \text{and Ba}$) phosphors. The fact that the PL intensities of the two phosphors (for Ca and Sr) remarkably enhanced after N^{3-} doping, whereas that of $\text{Li}_2\text{BaSiO}_4:\text{Eu}^{2+}$ is not changed, corroborates the structural strain effect on the PL intensity (see Figure 7). Furthermore, the structural strain effect by the N^{3-} doping prominently appears in UV–visible absorbance spectra (see Figure 9). Evidently, for Ca and Sr, the stronger absorption bands between 300 and 500 nm are present after N^{3-} doping, while for Ba, the absorption bands are nearly same before and after N^{3-} doping. Presumably, the compressive strain plays an important role in the effective transfer of the absorbed energy from the host lattice to the activator ion even though the difference of strain values before and after N^{3-} doping is very small, resulting in the enhanced absorption band and PL intensity.

Photoluminescence of LEDs. To examine the potential of the as-synthesized phosphors for near-UV LED application,

phosphor-converted LEDs were made using a phosphor powder and a InGaN LED with 365 nm emission. Figure 12 shows the emission spectra of $\text{Li}_2\text{MSiO}_4:\text{Eu}^{2+}$ ($\text{M} = \text{Ca}, \text{Sr}, \text{and Ba}$) phosphors before and after N^{3-} doping using an InGaN LED ($\lambda_{\text{max}} = 365 \text{ nm}$) under forward-bias currents from 10 to 50 mA. Figure 12 clearly shows that the 365 nm UV light emitted from the InGaN chip is absorbed by the phosphors and simultaneously downconverted into intensive, wide-band-emitting light. Upon increasing the forward-bias current from 10 to 50 mA, the emission intensities of the phosphors progressively increase. At the same time, the luminous output increases and the shape and position of the LED emission bands exhibit similarity, thus confirming that the phosphors show a stable emission property. As presented in Figure 12, the maximum LED emission intensity for Ca and Sr increases after N^{3-} doping, which is consistent with the PL spectra (see Figure 7). For a white LED, the N^{3-} -doped $\text{Li}_2\text{MSiO}_{4-\delta}\text{N}_{2/3\delta}:\text{Eu}^{2+}$ ($\text{M} = \text{Ca}, \text{Sr}, \text{and Ba}$) phosphors were mixed and monitored using a color coordinate meter to determine the appropriate mixing proportions. The appropriate mixing proportions were determined as 46.7 wt % Ca, 46.6 wt % Sr, and 6.7 wt % Ba. Figure 13 presents the CIE

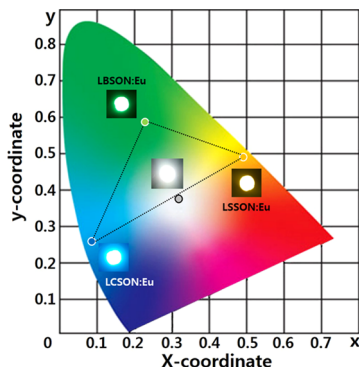


Figure 13. CIE chromaticities of LCSON:Eu, LSSON:Eu, LBSO:N:Eu, and the mixed powder with three phosphors monitored under 365 nm UV light.

chromaticity of LEDs monitored under a forward-bias current of 50 mA. The N^{3-} -doped $\text{Li}_2\text{CaSiO}_{4-\delta}\text{N}_{2/3\delta}:\text{Eu}^{2+}$ emits blue light with the (0.090, 0.253) chromaticity coordinate. The N^{3-} -doped $\text{Li}_2\text{SrSiO}_{4-\delta}\text{N}_{2/3\delta}:\text{Eu}^{2+}$ emits yellow light with the (0.496, 0.495) chromaticity coordinate. The N^{3-} -doped $\text{Li}_2\text{BaSiO}_{4-\delta}\text{N}_{2/3\delta}:\text{Eu}^{2+}$ emits green light with the (0.241, 0.584) chromaticity coordinate. Finally, the white zone formed by mixing the light from the three phosphors corresponds to the (0.333, 0.373) chromaticity coordinate, a color-rendering index of $R_a = 83$, and correlated color temperature of 5480 K.

CONCLUSIONS

In this work, $\text{Li}_2\text{MSiO}_4:\text{Eu}^{2+}$ ($\text{M} = \text{Ca}, \text{Sr}, \text{and Ba}$) phosphors before and after N^{3-} doping were systematically prepared and analyzed. SIMS measurement revealed that the average contents of N^{3-} ion for LCSON, LSSON, and LBSO were 0.003, 0.009, and 0.032, respectively, probably implying that $\text{Li}_2\text{MSiO}_{4-\delta}\text{N}_{2/3\delta}:\text{Eu}^{2+}$ ($\text{M} = \text{Ca}, \text{Sr}, \text{and Ba}$) phosphors with larger ion size can easily accommodate more N^{3-} ions in the crystal lattice sites. Furthermore, the N^{3-} sited in the host lattices was corroborated by IR and XPS analyses, i.e., the chemical shift of Si–O stretching mode from 825 to 817 cm^{-1} after N^{3-} doping (for LSSON) and the chemical shift of Si 2p

binding energy from 101.5 to 100.7 eV and the presence of the N 1s binding energy at 393.4 eV after N^{3-} doping (for LSSON). From the PL spectra in $\text{Li}_2\text{MSiO}_4:\text{Eu}^{2+}$ ($\text{M} = \text{Ca}, \text{Sr}, \text{and Ba}$) phosphors before and after N^{3-} doping, it was verified that the enhanced emission intensity of the phosphors is most likely due to N^{3-} doping. The change of the emission band maxima was also investigated in these phosphors. In $\text{Li}_2\text{MSiO}_4:\text{Eu}^{2+}$ ($\text{M} = \text{Ca}, \text{Sr}, \text{and Ba}$) phosphors, the maximum wavelengths of the emission bands were red-shifted in the order $\text{Ca} < \text{Ba} < \text{Sr}$, which is not consistent with the trend of crystal field splitting: $\text{Ba} < \text{Sr} < \text{Ca}$. This discrepancy between the shift of emission band maxima and trend based on the crystal field splitting was clearly explained by electron–electron repulsions among polyhedra, LiO_4MO_n , SiO_4MO_n , and $\text{MO}_n\text{M}'\text{O}_n$ associated with structural difference in host lattices. Therefore, the energy levels associated with the $4f^6\text{Sd} \rightarrow 4f^7$ transition of Eu^{2+} are definitely established in the following order: $\text{Li}_2\text{CaSiO}_4:\text{Eu}^{2+} > \text{Li}_2\text{BaSiO}_4:\text{Eu}^{2+} > \text{Li}_2\text{SrSiO}_4:\text{Eu}^{2+}$. Furthermore, using Williamson–Hall (W–H) method, the determined structural strains of $\text{Li}_2\text{MSiO}_4:\text{Eu}^{2+}$ ($\text{M} = \text{Ca}, \text{Sr}, \text{and Ba}$) phosphors revealed that the increased compressive strain after N^{3-} doping plays an important role in the enhanced PL intensity of these phosphors. White LEDs fabricated by a combination of three N^{3-} -doped phosphors and a 365 nm emitting InGaN chip exhibited the (0.333, 0.373) color coordinate and a high color-rendering index ($R_a = 83$). These phosphor materials may provide a platform for development of new efficient phosphors in solid-state lighting field.

EXPERIMENTAL SECTION

$\text{Li}_2\text{MSiO}_4:\text{Eu}^{2+}$ ($\text{M} = \text{Ca}, \text{Sr}, \text{and Ba}$) phosphors were prepared from a stoichiometric mixture of MCO_3 ($\text{M} = \text{Ca}, \text{Sr}, \text{and Ba}$), SiO_2 , Li_2CO_3 , and Eu_2O_3 under a reducing atmosphere (4% H_2/Ar) at 900 °C for 12 h. N^{3-} -doped $\text{Li}_2\text{MSiO}_{4-\delta}\text{N}_{2/3\delta}:\text{Eu}^{2+}$ ($\text{M} = \text{Ca}, \text{Sr}, \text{and Ba}$) phosphors were prepared from a stoichiometric mixture of MCO_3 ($\text{M} = \text{Ca}, \text{Sr}, \text{and Ba}$), $\alpha\text{-Si}_3\text{N}_4$, Li_2CO_3 , and Eu_2O_3 under NH_3 atmosphere at 900 °C for 12 h. The Eu^{2+} ion concentration was fixed at 1 mol %. X-ray diffraction analysis was carried out using a graphite monochromator (DMAX-2200PC, Rigaku). A step scan mode was selected in a 2θ range (10–110°) with a step size of 0.02° and counting time of 5 s for each step. The refinements of crystal structure were carried out by the Rietveld method using the FullProf program. The diffraction profiles were fitted using a pseudo-Voigt peak function and manually selected background points. FT-IR analyses were carried out using a Bruker VERTEX70 FT-IR spectrometer with an extension in the far-IR region. The extension consists of a multilayer mylar beam splitter, a room-temperature DLATGS detector with preamplifier, and polyethylene windows for the internal optical path. The binding energies of the elements were determined by an X-ray photoelectron spectrophotometer (ESCALAB 250) with a monochromatic $\text{Al K}\alpha$ X-ray source ($h\nu = 1486.6 \text{ eV}$) at Busan Center of Korea Basic Science Institute (KBSI). The determined binding energies were calibrated using the internal standard of adventitious carbon (C 1s at 284.6 eV). SIMS (CAMECA IMS-6f, France) was carried out to determine the elemental composition of the N^{3-} -substituted phosphors. The SIMS standard was used with ${}^{14}\text{N}$ isotope implanted into SiO_2 film as N^+ at 100 keV (a dose of $5 \times 10^{14} \text{ ions/cm}^2$). To determine the relative sensitivity factor (RSF) of each element, the intensity of secondary ion was corrected by the SIMS

results from the standard material. For a careful examination, the Cs^+ primary-ion beam was focused using an electron neutralizer for charge compensation (net impact energy = 15 keV; beam current = 20 nA). The PL spectra were obtained using a fluorometer (FS-2 model, Scinco) with a xenon lamp (150 W) under an operating voltage of 350 V. The diffuse reflectance spectra were obtained using a UV-visible spectrophotometer (UV-2600, Shimadzu) with a BaSO_4 reference.

■ ASSOCIATED CONTENT

Supporting Information

The Supporting Information is available free of charge on the ACS Publications website at DOI: [10.1021/acsomega.8b03489](https://doi.org/10.1021/acsomega.8b03489).

Rietveld refinement results, selected bond lengths of $\text{Li}_2\text{MSiO}_4:\text{Eu}$ ($\text{M} = \text{Ca}, \text{Sr}, \text{and Ba}$) materials (Tables S1–S6); and FT-IR spectra of MCO_3 ($\text{M} = \text{Ca}, \text{Sr}, \text{and Ba}$) (Figure S1) ([PDF](#))

■ AUTHOR INFORMATION

Corresponding Authors

*E-mail: sjookim@ajou.ac.kr (S.-J. Kim).
*E-mail: parkjc@silla.ac.kr (J.-C. Park).

ORCID

Donghyeon Kim: [0000-0003-0376-3356](https://orcid.org/0000-0003-0376-3356)

In Chung: [0000-0001-6274-3369](https://orcid.org/0000-0001-6274-3369)

Seung-Joo Kim: [0000-0002-9945-5181](https://orcid.org/0000-0002-9945-5181)

Jung-Chul Park: [0000-0002-0573-018X](https://orcid.org/0000-0002-0573-018X)

Present Address

[#]Department of Advanced Materials Engineering, Korea Polytechnic University, Gyeonggi 15073, Republic of Korea (C.W. Ji).

Notes

The authors declare no competing financial interest.

■ ACKNOWLEDGMENTS

This research was supported by Basic Science Research Program through the National Research Foundation of Korea (NRF) funded by the Ministry of Education (Grant 2017R1D1A1B03034550). S.-J. Kim, one of the authors, acknowledges the partial support by the GRRC program of Gyeonggi province (GRRC-Ajou- 2016B02).

■ REFERENCES

- (1) Lin, C. C.; Liu, R.-S. Advances in phosphors for light-emitting diodes. *J. Phys. Chem. Lett.* **2011**, *2*, 1268–1277.
- (2) Kim, D.; Jeon, K.-W.; Jin, J. S.; Kang, S.-G.; Seo, D.-K.; Park, J.-C. Remarkable flux effect of Li-codoping on highly enhanced luminescence of orthosilicate $\text{Ba}_3\text{SiO}_4:\text{Eu}^{2+}$ phosphors for NUV-LEDs: autonomous impurity purification by eutectic Li_2CO_3 melts. *RSC Adv.* **2015**, *5*, 105339–105346.
- (3) Kim, D.; Bae, J.-S.; Hong, T. E.; Hui, K. N.; Kim, S.; Kim, C. H.; Park, J.-C. Color-Tunable and Highly Luminous N^{3-} -Doped $\text{Ba}_{2-x}\text{Ca}_x\text{SiO}_{4-\delta}\text{N}_{2/3\delta}:\text{Eu}^{2+}$ ($0.0 \leq x \leq 1.0$) Phosphors for White NUV-LED. *ACS Appl. Mater. Interfaces* **2016**, *8*, 17371–17381.
- (4) Woo, H.-J.; Gandhi, S.; Cho, K.; Shin, D.-S.; Yi, S. S.; Jeong, J. H.; Jang, K. Facile preparation of silicate phosphor activated with low concentration of Eu^{2+} ions for highly efficient warm white light production. *Ceram. Int.* **2016**, *42*, 13301–13304.
- (5) Zhang, X.; Dong, Z.; Shi, J.; Gong, M. Luminescence properties of color-tunable zinc-codoped alkali earth sulfide phosphor for LED application. *Mater. Lett.* **2012**, *76*, 113–116.
- (6) Wang, X.-M.; Wang, C.-H.; Kuang, X.-J.; Zou, R.-Q.; Wang, Y.-X.; Jing, X.-P. Promising oxonitridosilicate phosphor host $\text{Sr}_3\text{Si}_2\text{O}_4\text{N}_2$: Synthesis, structure, and luminescence properties activated by Eu^{2+} and $\text{Ce}^{3+}/\text{Li}^+$ for pc-LEDs. *Inorg. Chem.* **2012**, *51*, 3540–3547.
- (7) Liu, T.-C.; Cheng, B.-M.; Hu, S.-F.; Liu, R.-S. Highly stable red oxynitride $\beta\text{-SiAlON:Pr}^{3+}$ phosphor for light-emitting diodes. *Chem. Mater.* **2011**, *23*, 3698–3705.
- (8) George, N. C.; Birkel, A.; Brgoch, J.; Hong, B.-C.; Mikhailovsky, A. A.; Page, K.; Llobet, A.; Seshadri, R. Average and Local Structural Origins of the Optical Properties of the Nitride Phosphor $\text{La}_{3-x}\text{Ce}_x\text{Si}_6\text{N}_{11}$ ($0 < x \leq 3$). *Inorg. Chem.* **2013**, *52*, 13730–13741.
- (9) Liu, J.; Sun, J.; Shi, C. A new luminescent material: $\text{Li}_2\text{CaSiO}_4:\text{Eu}^{2+}$. *Mater. Lett.* **2006**, *60*, 2830–2833.
- (10) Saradhi, M. P.; Varadaraju, U. Photoluminescence studies on Eu^{2+} -activated $\text{Li}_2\text{SrSiO}_4$ a potential orange-yellow phosphor for solid-state lighting. *Chem. Mater.* **2006**, *18*, 5267–5272.
- (11) Kulshreshtha, C.; Shin, N.; Sohn, K.-S. Decay behavior of $\text{Li}_2(\text{Sr}, \text{Ba}, \text{Ca})\text{SiO}_4$: Eu^{2+} Phosphors. *Electrochem. Solid-State Lett.* **2009**, *12*, J55–J57.
- (12) Kim, J.; Ahn, D.; Kulshreshtha, C.; Sohn, K.-S.; Shin, N. Lithium barium silicate, $\text{Li}_2\text{BaSiO}_4$ from synchrotron powder data. *Acta Crystallogr., Sect. C: Cryst. Struct. Commun.* **2009**, *65*, i14–i16.
- (13) Li, Y.; Delsing, A.; De With, G.; Hintzen, H. Luminescence properties of Eu^{2+} -activated alkaline-earth silicon-oxynitride $\text{MSi}_2\text{O}_{2-\delta}\text{N}_{2+2/3\delta}$ ($\text{M} = \text{Ca}, \text{Sr}, \text{Ba}$): a promising class of novel LED conversion phosphors. *Chem. Mater.* **2005**, *17*, 3242–3248.
- (14) Gu, Y.; Zhang, Q.; Li, Y.; Wang, H. Simultaneous tuning for excitation and emission of N doped $\text{Sr}_2\text{SiO}_4:\text{Eu}$ for white light LEDs. *J. Alloys Compd.* **2011**, *509*, L109–L112.
- (15) Fang, Y.; Li, Y.; Xie, R.; Hirosaki, N.; Takade, T.; Li, X.; Qiu, T. Structure and photoluminescence properties of Ce^{3+} -doped novel silicon-oxynitride $\text{Ba}_{4-z}\text{M}_z\text{Si}_8\text{O}_{20-3z}\text{N}_{2z}$ ($\text{M} = \text{Mg}, \text{Ca}, \text{Sr}$). *J. Solid State Chem.* **2011**, *184*, 1405–1414.
- (16) Chen, W.-T.; Sheu, H.-S.; Liu, R.-S.; Attfield, J. P. Cation-size-mismatch tuning of photoluminescence in oxynitride phosphors. *J. Am. Chem. Soc.* **2012**, *134*, 8022–8025.
- (17) Huheey, J. E.; Keiter, E. A.; Keiter, R. L. *Inorganic Chemistry: Principles of Structure and Reactivity*; Harper Collins College Publishers: New York, 1993.
- (18) Song, K.; Zhang, F.; Chen, D.; Wu, S.; Zheng, P.; Huang, Q.; Jiang, J.; Xu, J.; Qin, H. Enhancement of photoluminescence properties and modification of crystal structures of Si_3N_4 doping $\text{Li}_2\text{Sr}_{0.995}\text{SiO}_4:0.005\text{Eu}^{2+}$ phosphors. *Mater. Res. Bull.* **2015**, *70*, 309–314.
- (19) Rietveld, H. A profile refinement method for nuclear and magnetic structures. *J. Appl. Crystallogr.* **1969**, *2*, 65–71.
- (20) Rodríguez-Carvajal, J. Recent Developments of the Program FULLPROF Commission on Powder Diffraction (IUCr). *Newsletter* **2001**, *26*, 12–19.
- (21) Walker, A. V. Why is SIMS Underused in Chemical and Biological Analysis? Challenges and Opportunities. *Anal. Chem.* **2008**, *80*, 8865–8870.
- (22) Seki, S.; Tamura, H.; Sumiya, H. Quantitative SIMS analysis of nitrogen using in situ internal implantation. *Appl. Surf. Sci.* **1999**, *147*, 14–18.
- (23) Scott, J.; Porto, S. Longitudinal and transverse optical lattice vibrations in quartz. *Phys. Rev.* **1967**, *161*, No. 903.
- (24) Etchepare, J.; Merian, M.; Smetankine, L. Vibrational normal modes of SiO_2 . I. α and β quartz. *J. Chem. Phys.* **1974**, *60*, 1873–1876.
- (25) Ocaña, M.; Fornés, V.; García-Ramos, J. V.; Serna, C. Polarization effects in the infrared spectra of α -quartz and α -cristobalite. *Phys. Chem. Miner.* **1987**, *14*, 527–532.
- (26) Handke, M.; Urban, M. IR and Raman spectra of alkaline earth metals orthosilicates. *J. Mol. Struct.* **1982**, *79*, 353–356.

- (27) Pires, A. M.; Davolos, M. R. Luminescence of europium (III) and manganese (II) in barium and zinc orthosilicate. *Chem. Mater.* **2001**, *13*, 21–27.
- (28) Batsanov, S. Dependence of energies on the bond lengths in molecules and crystals. *J. Struct. Chem.* **2008**, *49*, 296–303.
- (29) Shluger, A. On the nonequivalency of Si-O bonds in silicon dioxide. *J. Phys. Chem. Solids* **1986**, *47*, 659–664.
- (30) Matsunaga, K.; Iwamoto, Y. Molecular dynamics study of atomic structure and diffusion behavior in amorphous silicon nitride containing boron. *J. Am. Ceram. Soc.* **2001**, *84*, 2213–2219.
- (31) Luo, Y.-R. *Comprehensive Handbook of Chemical Bond Energies*; CRC Press: Boca Raton, FL, 2007.
- (32) Pauling, L. The principles determining the structure of complex ionic crystals. *J. Am. Chem. Soc.* **1929**, *51*, 1010–1026.
- (33) Morrison, C. A. Host dependence of the rare-earth ion energy separation $4f^N - 4f^{N-1}$ nl. *J. Chem. Phys.* **1980**, *72*, 1001–1002.
- (34) Shi, J. S.; Zhang, S. Y. Barycenter of Energy of Lanthanide $4f^{N-1}5d$ Configuration in Inorganic Crystals. *J. Phys. Chem. B* **2004**, *108*, 18845–18849.
- (35) Setyawan, W.; Gaume, R. M.; Lam, S.; Feigelson, R. S.; Curtarolo, S. High-throughput combinatorial database of electronic band structures for inorganic scintillator materials. *ACS Comb. Sci.* **2011**, *13*, 382–390.
- (36) Alemi, A.; Khademina, S.; Joo, S. W.; Dolatyari, M.; Bakhtiari, A. Lithium metasilicate and lithium disilicate nanomaterials: optical properties and density functional theory calculations. *Int. Nano Lett.* **2013**, *3*, No. 14.
- (37) Asami, K.; Ueda, J.; Yasuda, K.; Hongo, K.; Maezono, R.; Brik, M. G.; Tanabe, S. Development of persistent phosphor of Eu²⁺ doped Ba₂SiO₄ by Er³⁺ codoping based on vacuum referred binding energy diagram. *Opt. Mater.* **2018**, *84*, 436–441.
- (38) Williamson, G. K.; Hall, W. H. X-ray line broadening from filed aluminium and wolfram. *Acta Metall.* **1953**, *1*, 22–31.
- (39) Feng, I. W.; Li, J.; Sedhain, A.; Lin, J. Y.; Jiang, H. X.; Zavada, J. Enhancing erbium emission by strain engineering in GaN heteroepitaxial Layers. *Appl. Phys. Lett.* **2010**, *96*, No. 031908.
- (40) Singh, L. P.; Singh, N. P.; Singh, T. D. Enhancement of Luminescence Intensity in Dy³⁺ Ions Doped YVO₄ Nanomaterials by Ba²⁺ Ion Codoping and YVO₄:2Dy/Fe₃O₄ Nanohybrid for Hyperthermia Application. *J. Nanomed. Nanotechnol.* **2017**, *8*, No. 1000445.
- (41) Yang, Q.; Wang, W.; Xu, S.; Wang, Z. L. Enhancing Light Emission of ZnO Microwire-Based Diodes by Piezo-Phototronic Effect. *Nano Lett.* **2011**, *11*, 4012–4017.